Soft Matter

PAPER

View Article Online
View Journal | View Issue

Cite this: *Soft Matter*, 2020, **16**, 1518

Memory-induced motion reversal in Brownian liquids

Lucas L. Treffenstädt and Matthias Schmidt *

Received 8th October 2019,
Accepted 7th January 2020

DOI: 10.1039/c9sm02005e

rsc.li/soft-matter-journal

We study the Brownian dynamics of hard spheres under spatially inhomogeneous shear, using event-driven Brownian dynamics simulations and power functional theory. We examine density and current profiles both for steady states and for the transient dynamics after switching on and switching off an external square wave shear force field. We find that a dense hard sphere fluid (volume fraction ≈ 0.35) undergoes global motion reversal after switching off the shear force field. We use power functional theory with a spatially nonlocal memory kernel to describe the superadiabatic force contributions and obtain good quantitative agreement of the theoretical results with simulation data. The theory provides an explanation for the motion reversal: internal superadiabatic nonequilibrium forces that oppose the externally driven current arise due to memory after switching off. The effect is genuinely viscoelastic: in steady state, viscous forces oppose the current, but they elastically generate an opposing current after switch-off.

I. Introduction

The non-equilibrium properties of hard spheres under shear have attracted considerable attention. Rheological experiments under steady shear, *e.g.* using silica particles,[1,2] show non-Newtonian viscosity effects, with both shear thickening and shear thinning occurring depending on the volume fraction. Shear thinning was observed in Brownian dynamics (BD) simulation, *e.g.* by Foss and Brady.[3] Dhont *et al.* studied the distortion of the microstructure of colloids using light scattering experiments.[4] Dhont and Nägele derived the viscoelastic response of a suspension of colloids to shear from the Smoluchowski equation.[5] Fuchs and coworkers have developed theoretical descriptions of these effects using mode coupling theory and integration through transients.[6–8] A thorough overview of the nonlinear rheology of colloidal dispersions has been given by Brader.[9]

Hard spheres under inhomogeneous shear exhibit a broad range of effects. In particular, inhomogeneities in the shear rate can induce particle migration[10] and thus lead to inhomogeneities in the density profile. Examples of this mechanism are lane formation, where particles move in stacked layers separated by low density bands,[11,12] and deformation of boundary density profiles of sheared systems in confinement.[13–15] Jin *et al.* studied flow instabilities in inhomogeneous shear with Browninan dynamics simulations.[16]

The transient behaviour in the time evolution from equilibrium to a sheared steady state and the reverse process from steady shear to equilibrium has attracted similar attention. Reinhardt *et al.*[17] studied the distortion of the pair correlation function under start-up shear. Koumakis *et al.*[18] reported on stresses in the start-up phase of shearing, in particular on the dependence of the stress overshoot on the Peclet number and on the volume fraction, using both simulation and experiments with sterically stabilized PMMA spheres using confocal microscopy and rheological measurements. Stress overshoot in start-up and cessation of shear and the connection to the microscopic fluid structure have also been studied.[19] Ackerson *et al.*[20] reported on solid-like ordering of nearly hard spheres under the influence of oscillatory shear. Krüger and Brader applied dynamic density functional theory,[21,22] extended to sheared systems with a scattering kernel approach,[13] to study sedimentation of colloids under time-dependent shear,[23] and Metzger and Butler examined the time evolution of particle clusters in periodic shear.[24]

Microscopic methods such as BD or molecular dynamics simulations are based on equations of motions which are instantaneous in time on the many-body level. However, on the one-body level, nonequilibrium states are generally dependent on the history of the system. By integrating out degrees of freedom, coarse-grained methods can be obtained, which generally have non-Markovian form, as can be shown with the Mori–Zwanzig formalism.[25,26] There is previous work done to derive accurate memory kernels for generalised Langevin equations for Brownian dynamics. Smith and Harris[27] proposed a method to approximate memory kernels and generate random

Theoretische Physik II, Universität Bayreuth, Universitätsstr. 30, D-95447 Bayreuth, Germany. E-mail: Matthias.Schmidt@uni-bayreuth.de

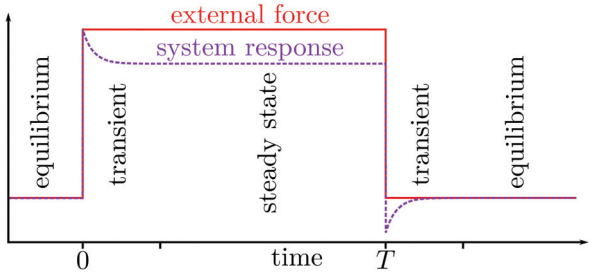

Fig. 1 Sketch of the time evolution of the system, external force (solid red line) and system response (dashed purple line) in arbitrary units. The system was in equilibrium at negative times. An external force is switched on at $t = 0$, and the system is monitored during the transient into a steady state as well as in the steady state itself. At time $t = T$, the external force is switched off and the system is observed until it has reached equilibrium again.

forces with a given autocorrelation. Szymczak and Cichocki[28] studied memory in the macroscopic dynamics of Brownian systems. Bao *et al.*[29] investigated breaking of ergodicity due to memory in non-Markovian Brownian dynamics. Recently, iterative methods have been developed to reconstruct memory kernels for generalized Langevin equations from molecular dynamics simulations by matching the force autocorrelation function or the velocity autocorrelation function between both methods.[30,31]

In this paper, we examine a system of Brownian hard spheres both in steady state under temporally constant but spatially inhomogeneous shear as well as the transient dynamics after switching the driving field both on and off. Fig. 1 shows a sketch of the dynamics: starting in a well-defined equilibrium state, a shear force field is switched on. The system needs some time to relax into a steady state. Then, the shear force field is switched off, and the system relaxes back into equilibrium. We report in particular on the shape of the current profile in the steady state under the influence of a square wave shear profile. This particular form of shear is well suited to show and examine nonlocal effects, since small regions of extreme shear rate alternate with large regions of low shear rate. We find that the transition in the current field between opposite flow directions is non-monotonic. After switching-off of the driving shear force, the current field reverses globally before settling into equilibrium.

We employ state-of-the-art event driven Brownian dynamics simulations,[32] which solve the problem of infinite gradients in the hard sphere interaction potential by evolving the system continuously with ballistic motion between BD timesteps. At fixed timesteps, the velocities of the particles are randomised according to a Maxwell distribution.

In addition to observations in simulation, the system is examined in the framework of power functional theory (PFT),[33] which describes the full non-equilibrium dynamics of many-particle systems, beyond the adiabatic approximation made in dynamical density functional theory (DDFT). DDFT is an extension of equilibrium density functional theory (DFT) to nonequilibrium systems,[34,35] which approximates the time evolution of the system through a series of adiabatic states, where the internal forces can be calculated from an equivalent equilibrium system with matching instantaneous density.[36] However, this approximation leads to shortcomings, such as underestimation of relaxation times.[34] There have been attempts to correct these shortcomings *via* empirical corrections, see *e.g.* ref. 37 and 38.

Superadiabatic forces were shown to occur in a variety of systems, such as Gaussian core particles,[39] hard spheres[40] and active Brownian particles.[41] We extend here an approximation for superadiabatic forces for Brownian hard spheres, presented recently by de las Heras and Schmidt[40] by introducing a diffusing memory kernel. This approximation derives forces from the gradient of the velocity field. The free parameters in this model – memory time, memory diffusion constant, and overall memory strength – are determined using a least-squares fit to BD simulation data.

This paper is organised as follows: in Section II, we introduce the considered system and our PFT approach. Section III contains implementation details for the BD simulations. Sections IV and V cover results in steady state and during transients, respectively. We draw conclusions and provide an outlook in Section VI.

II. Model and power functional theory

We consider a fluid of N monodisperse hard spheres with diameter σ. The system has planar geometry with Cartesian coordinates $\mathbf{r} = (x,y,z)$ and we take σ as the unit of length. Isotropy is broken by an external shear force field

$$\mathbf{f}_{\text{ext}}(\mathbf{r}) = f_{\text{ext}}(x)\hat{\mathbf{e}}_z, \tag{1}$$

where $\hat{\mathbf{e}}_z$ is the unit vector in the z-direction and $f_{\text{ext}} = |\mathbf{f}_{\text{ext}}|$ is the modulus of the force field. Since the intrinsic dynamics are diffusive, we choose as the unit of time the diffusion time $\tau = \sigma^2/D$ with diffusion constant $D = k_{\text{B}}T/\gamma$, where k_{B} is the Boltzmann constant, T indicates the absolute temperature, and γ is the friction constant against the implicit solvent.

The particle positions $\mathbf{r}_1,\ldots,\mathbf{r}_N \equiv \mathbf{r}^N$ evolve in time according to the Langevin equation of motion

$$\gamma\dot{\mathbf{r}}_i(t) = \mathbf{f}_{\text{int},i}(\mathbf{r}^N) + \mathbf{f}_{\text{ext}}(\mathbf{r}_i,t) + \sqrt{2\gamma k_{\text{B}}T}\mathbf{R}_i(t) \tag{2}$$

where $\mathbf{f}_{\text{int},i} = -\nabla_i u(\mathbf{r}^N)$ is the internal force that all other particles exert on particle i due to the interaction potential $u(\mathbf{r}^N)$ and $\mathbf{R}_i(t)$ is a delta-correlated Gaussian random white noise with $\langle\mathbf{R}_i(t)\rangle = 0$ and $\langle\mathbf{R}_i(t)\mathbf{R}_j(t')\rangle = \delta(t-t')\delta_{ij}\mathbb{1}$, where $\delta(\cdot)$ is the Dirac distribution, δ_{ij} indicates the Kronecker delta, and $\mathbb{1}$ is the 3×3 unit matrix.

The one-body density distribution is defined as

$$\rho(\mathbf{r},t) = \left\langle \sum_i \delta(\mathbf{r}-\mathbf{r}_i) \right\rangle, \tag{3}$$

where $\langle\cdot\rangle$ indicates an average over the noise and over initial microstates. The one-body current distribution is defined as

$$\mathbf{J}(\mathbf{r},t) = \left\langle \sum_i \delta(\mathbf{r}-\mathbf{r}_i)\mathbf{v}_i(t) \right\rangle, \tag{4}$$

where, in a numerical simulation, $\mathbf{v}_i$ must be calculated with a finite difference centred at time t.[42] The velocity field $\mathbf{v}(\mathbf{r},t)$ is defined as

$$\mathbf{v}(\mathbf{r},t) = \frac{\mathbf{J}(\mathbf{r},t)}{\rho(\mathbf{r},t)}. \tag{5}$$

The dynamics of (3) and (4) can be expressed as

$$\gamma\mathbf{v}(\mathbf{r},t) = \mathbf{f}_{\text{int}} + \mathbf{f}_{\text{ext}} - k_{\text{B}}T\nabla\ln\rho, \tag{6}$$

$$\frac{\partial}{\partial t}\rho(\mathbf{r},t) = -\nabla\cdot\mathbf{J}(\mathbf{r},t), \tag{7}$$

with the total internal one-body force field given by the configurational average

$$\mathbf{f}_{\text{int}}(\mathbf{r},t) = \frac{1}{\rho}\left\langle\sum_i \delta(\mathbf{r}-\mathbf{r}_i)\mathbf{f}_{\text{int},i}\right\rangle. \tag{8}$$

Eqn (6) constitutes the one-body force balance relationship where the negative friction force (left hand side) is equal to the sum of internal, external and diffusive one-body forces (right hand side). The one-body continuity equation (7) is a consequence of local particle conservation and it links the density profile and the current distribution to each other. The set of equations (6) and (7) is exact and can be obtained from averaging over the many-body Smoluchowski equation (see, *e.g.*, ref. 33).

The internal force field consists of two parts according to

$$\mathbf{f}_{\text{int}} = \mathbf{f}_{\text{ad}} + \mathbf{f}_{\text{sup}}, \tag{9}$$

with the adiabatic force ($\mathbf{f}_{\text{ad}}$) and the superadiabatic force ($\mathbf{f}_{\text{sup}}$) contributions.[33,36] The adiabatic force is defined as the internal force acting in a constructed equilibrium system with an external potential $V_{\text{ad}}(\mathbf{r})$ chosen such that the equilibrium density matches the instantaneous density $\rho(\mathbf{r},t)$. The underlying map from the equilibrium density distribution to the external potential V_{ad} has been shown by Evans[43] and Mermin.[44] Thus, $\mathbf{f}_{\text{ad}}$ depends only on the density at time t.

The superadiabatic force field, in contrast, depends in general on the history of both $\rho(\mathbf{r},t')$ and $\mathbf{J}(\mathbf{r},t')$ for $t' \le t$, making (6) in general an implicit equation. This distinction physically defines the splitting of internal forces. Superadiabatic forces can be measured in particle-based simulations[36] and they are absent in dynamical density functional theory.[34,35]

Power functional theory is based on the free power functional $R_t[\rho, \mathbf{J}]$, which captures in a formally exact way the full many-body dynamics. R_t is microscopically defined[33] and it satisfies an instantaneous minimisation principle with respect to the current. As a result, the functional derivative with respect to the current distribution vanishes at the minimum,

$$\frac{\delta R_t[\rho,\mathbf{J}]}{\delta\mathbf{J}(\mathbf{r},t)} = 0 \quad (\text{min}), \tag{10}$$

where the density is held fixed upon building the derivative. The functional dependence of $R_t[\rho, \mathbf{J}]$ is also on the history of the system, *i.e.* on $\rho(\mathbf{r},\tilde{t})$ and $\mathbf{J}(\mathbf{r},\tilde{t})$ for $\tilde{t} < t$. Eqn (10) determines the current $\mathbf{J}(\mathbf{r},t)$ at time t, which then allows together with the continuity eqn (7) to evolve the system in time.

The free power functional $R_t[\rho,\mathbf{J}]$ consists of a sum of intrinsic and external contributions.[33] The intrinsic contribution is composed of an adiabatic part that is the time derivative of the adiabatic free energy ($\dot{F}$) and a superadiabatic part (P_t) which is the genuine nonequilibrium contribution. Both are combined together with the external power X_t *via*[33]

$$R_t = \dot{F} + P_t - X_t. \tag{11}$$

Inserting the decomposition (11) in the condition (10) and carrying out the functional derivatives leads to the force balance relation (6). In order to illustrate this, we briefly describe all occurring terms; details can be found in ref. 33.

The time derivative of the intrinsic Helmholtz free energy functional $F[\rho]$ is given by

$$\dot{F} = \int\mathrm{d}\mathbf{r}\mathbf{J}\cdot\nabla\frac{\delta F[\rho]}{\delta\rho(\mathbf{r},t)}. \tag{12}$$

The (Helmholtz) free energy functional $F[\rho]$ consists of a sum of an ideal gas part and an excess contribution, $F_{\text{exc}}[\rho]$, which arises due to the interparticle interactions. Hence

$$F[\rho] = k_{\text{B}}T\int\mathrm{d}\mathbf{r}\rho[\ln(\rho\Lambda^3) - 1] + F_{\text{exc}}[\rho], \tag{13}$$

where the first term on the right hand side is the ideal gas free energy functional; Λ is the (irrelevant) thermal de Broglie wavelength. In the results presented below we choose the Rosenfeld functional[45] in order to approximate the excess free energy functional $F_{\text{exc}}[\rho]$ for hard spheres.

The (negative) functional derivative of $\dot{F}_{\text{exc}}$ with respect to $\mathbf{J}$ generates the adiabatic force field $\mathbf{f}_{ad}$ *via*

$$\mathbf{f}_{\text{ad}}(\mathbf{r},t) = -\frac{\delta\dot{F}_{\text{exc}}}{\delta\mathbf{J}(\mathbf{r},t)} = -\nabla\frac{\delta F_{\text{exc}}[\rho]}{\delta\rho(\mathbf{r},t)}. \tag{14}$$

As $F_{\text{exc}}[\rho]$ is a density functional and hence independent of the current, the adiabatic force field $\mathbf{f}_{\text{ad}}$ is also a functional of only the density profile ρ at time t.

The external power X_t, as it appears in the decomposition of the total free power (11), depends on the external force field $\mathbf{f}_{\text{ext}}$, as well as on the time derivative $\dot{V}_{\text{ext}}$ of the external potential. The external power is an instantaneous space integral over these one-body fields according to

$$X_t = \int\mathrm{d}\mathbf{r}(\mathbf{J}\cdot\mathbf{f}_{\text{ext}} - \rho\dot{V}_{\text{ext}}). \tag{15}$$

In the present application the external force field $\mathbf{f}_{\text{ext}}(\mathbf{r},t)$ is the sum of the shearing force field (1) and an additional conservative force field $-\nabla V_{\text{ext}}(\mathbf{r})$ which we use in order to induce particle migration effects. In the present application V_{ext} is independent of time and hence $\dot{V}_{\text{ext}} = 0$.

Finally, P_t consists of a sum of the ideal gas contribution (P_t^{id}) and an excess part (P_t^{exc}), according to

$$P_t = P_t^{\text{id}} + P_t^{\text{exc}}. \tag{16}$$

The ideal gas dissipation functional is given by the position- and time-local expression

$$P_t^{\mathrm{id}}[\rho,\mathbf{J}] = \gamma\int \mathrm{d}\mathbf{r}\frac{\mathbf{J}^2}{2\rho}. \tag{17}$$

The superadiabatic free power functional $P_t^{\mathrm{exc}}[\rho,\mathbf{J}]$ contains all genuine nonequilibrium effects that arise from the interparticle interactions. In general, its dependence on ρ and $\mathbf{J}$ is nonlocal in both space and in time, with the temporal dependence being of the "history", *i.e.* the behaviour at earlier times, as is clear from causality. The superadiabatic force field $\mathbf{f}_{\mathrm{sup}}$, *cf.* eqn (9), is generated *via* functional differentiation,

$$\mathbf{f}_{\mathrm{sup}}(\mathbf{r},t) = -\frac{\delta P_t^{\mathrm{exc}}[\rho,\mathbf{J}]}{\delta\mathbf{J}(\mathbf{r},t)}. \tag{18}$$

P_t^{exc} is specific to the type of interparticle interaction potential and must in general be approximated. This status is very similar to that of the excess free energy functional $F_{\mathrm{exc}}[\rho]$ in equilibrium DFT. Here, we choose the velocity gradient form,[40] given by

$$\begin{aligned} P_t^{\mathrm{exc}} = \frac{1}{2}\int \mathrm{d}\mathbf{r}\int \mathrm{d}\mathbf{r}'\int_{-\infty}^{t}\mathrm{d}t'\rho(\mathbf{r},t)[\eta(\nabla\times\mathbf{v})\cdot(\nabla'\times\mathbf{v}') \\ +\zeta(\nabla\cdot\mathbf{v})(\nabla'\cdot\mathbf{v}')]\rho(\mathbf{r}',t')K(\mathbf{r}-\mathbf{r}',t-t'), \end{aligned} \tag{19}$$

where $\mathbf{v} = \mathbf{v}(\mathbf{r},t)$ is the velocity field as defined in (5); we use the shorthand $\mathbf{v}' = \mathbf{v}(\mathbf{r}',t')$ to express dependence on the primed space and time arguments, and ∇' indicates the derivative with respect to $\mathbf{r}'$.

P_t^{exc} depends not only on the instantaneous density and velocity fields, but also on the history of the system, and it is non-local in space. The constants ζ and η indicate the volume viscosity and the shear viscosity, respectively. The coupling to the history is governed by the memory kernel $K(\mathbf{r}-\mathbf{r}',t-t')$. The kernel is normalised to unity, such that $\int\mathrm{d}\mathbf{r}\int\mathrm{d}tK(\mathbf{r},t) = 1$.

We consider two different functional forms of K. The first form, K_{L}, is chosen as a simple reference. It is taken to be local in space and to possess a purely exponential temporal decay:

$$K_{\mathrm{L}}(\mathbf{r},t) = \delta(\mathbf{r})\tau_{\mathrm{M}}^{-1}\exp(-t/\tau_{\mathrm{M}})\Theta(t), \tag{20}$$

with τ_{M} indicating the memory time and $\Theta(\cdot)$ denoting the Heaviside step function. We expect the form (20) to perform well in cases of small shear gradients, where it models time-dependent behaviour independent of spatial correlation effects.

The second version is spatially non-local. We base its functional form on the diffusive nature of the underlying microscopic dynamics. Hence we assume that that interactions between distant particles propagate according to an effective diffusion process, characterized by a corresponding memory diffusion constant D_{M}. Specifically we assume the memory kernel to possess the form

$$K_{\mathrm{D}}(\mathbf{r},t) = \frac{\mathrm{e}^{-\mathbf{r}^2/(4D_{\mathrm{M}}t)-t/\tau_{\mathrm{M}}}}{(4\pi D_{\mathrm{M}}t)^{3/2}\tau_{\mathrm{M}}}\Theta(t), \tag{21}$$

where the memory time τ_{M} sets the time scale for the decay, as above. We shall call the form (21) the diffusing memory kernel, since the spatial part corresponds to a diffusion process. The constants τ_{M} and D_{M} are adjustable parameters that in principle are determined by the underlying interparticle interactions.

The timescale τ_{M} controls the exponential decay of the memory effect. D_{M} has the units of (length)^2 per time and it controls how fast information propagates from point $\mathbf{r}'$ to point $\mathbf{r}$ in (19) *via* a diffusion process. In the limit of $t' \to t$, the spatial part of K_{D} approaches the Dirac delta distribution. Therefore, there are no instantaneous non-local interactions in this model.

In steady state, the density and the current do not depend on time, *i.e.* $\rho(\mathbf{r},t) = \rho_{\mathrm{s}}(\mathbf{r})$ and $\mathbf{J}(\mathbf{r},t) = \mathbf{J}_{\mathrm{s}}(\mathbf{r})$ with $\nabla\cdot\mathbf{J}_{\mathrm{s}} = 0$. In this case, the time integral in (19) acts only on K and, as K is known from (20) or (21), can be carried out explicitly. The respective results for both kernels are

$$K_{\mathrm{L}}^{\mathrm{s}} = \int_{-\infty}^{t}K_{\mathrm{L}}(\mathbf{r}-\mathbf{r}',t-t')\mathrm{d}t' = \delta(\mathbf{r}-\mathbf{r}'), \tag{22}$$

$$\begin{aligned} K_{\mathrm{D}}^{\mathrm{s}} &= \int_{-\infty}^{t}K_{\mathrm{D}}(\mathbf{r}-\mathbf{r}',t-t')\mathrm{d}t' \\ &= \frac{1}{4\pi\tau_{\mathrm{M}}D_{\mathrm{M}}|\mathbf{r}-\mathbf{r}'|}\exp\left(-\frac{|\mathbf{r}-\mathbf{r}'|}{\sqrt{\tau_{\mathrm{M}}D_{\mathrm{M}}}}\right). \end{aligned} \tag{23}$$

Thus, $K_{\mathrm{L}}^{\mathrm{s}}$ does not depend on the parameter τ_{M} and $K_{\mathrm{D}}^{\mathrm{s}}$ depends only on a new length scale

$$\sigma_{\mathrm{M}} = \sqrt{\tau_{\mathrm{M}}D_{\mathrm{M}}}, \tag{24}$$

which can be interpreted as an effective interaction length in steady state. The parameters τ_{M} and D_{M} can therefore not be independently determined from measurements of one-body quantities in steady state. However, one can determine the value of σ_{M}. In steady state, it is less computationally intensive to obtain accurate density and current profiles from particle simulations, so σ_{M} can be determined with high accuracy. Knowledge of σ_{M} then reduces the number of free parameters to be determined with measurements in the full time evolution.

For the given system, all integrals in y and z in $R_t[\rho,\mathbf{J}]$ can be explicitly carried out, since density and current are by construction homogeneous in these directions. Thus, the current only depends on one space coordinate x and time t: $\mathbf{J}(x,t) = J_x(x,t)\hat{\mathbf{e}}_x + J_z(x,t)\hat{\mathbf{e}}_z$, where J_x is the current in gradient direction $\hat{\mathbf{e}}_x$, and J_z is the current in flow direction $\hat{\mathbf{e}}_z$.

It should be noted that the form of P_t^{exc} applied here contains no coupling between the flow direction and the gradient direction of $\mathbf{J}$. Therefore, a system with an initially homogeneous density and no external force acting in the x direction will always remain homogeneous in this approximation, whereas in reality, structural migration forces occur. P_t^{exc} can be extended to include these effects,[39] but that is beyond the scope of this work. Instead, we impose the density profile ρ_{BD} obtained in BD simulations *via* an external potential $V_{\mathrm{ext}}(x)$, chosen so that $\rho_{\mathrm{BD}}(x)$ is the equilibrium density in the potential.

We numerically minimize $R_t[\rho,\mathbf{J}]$ for a given $\rho(x,t)$ at time t using a generic nonlinear numerical optimiser,[46] thus solving the Euler–Lagrange-eqn (10) and obtaining $\mathbf{J}(x,t)$. Using the continuity equation (7), we numerically evolve ρ in time, *i.e.* proceed by one time step Δt and repeat the procedure. Then, we compare results for $\rho(x,t)$ and

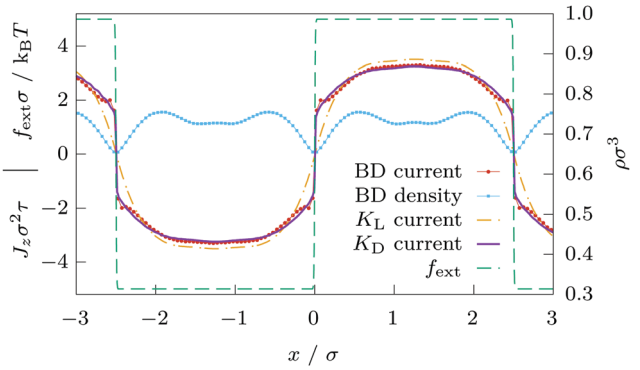

Fig. 2 Steady state current $J_z(x)$ and density profile $\rho(x)$ in BD simulation under a square wave shear force $f_{\mathrm{ext}}(x)$ acting along $\hat{\mathbf{e}}_z$. The plot shows only part of the simulation box.

$\mathbf{J}(x,t)$ calculated with PFT to results for the same quantities sampled in BD simulations. We determine the free parameters η, τ_{M}, and D_{M} that appear in P_t^{exc} [as given by (19) together with the alternative forms for the memory kernel (20) and (21)] by using a least-squares fit to the simulation results for the velocity field. Here the simulation results are obtained *via* sampling at fixed times during the transient time evolution. For steady states we average over time. We start from reasonable estimates for the parameters and use a nonlinear numerical optimiser[46] with a derivative-free optimisation routine.[47]

III. Brownian dynamics simulations

We employ event-driven Brownian dynamics simulations[32] to integrate the Langevin equation (2) and obtain particle trajectories. We use $N = 1090$ particles in a simulation box of size $10 \times 10 \times 15\ \sigma^3$ with periodic boundary conditions in all directions. By choosing a strongly inhomogeneous shear force field, we expect to clearly showcase the importance of nonlocal interactions. Our choice of a field that is periodic in x relieves us from the need for Lees–Edwards boundary conditions,[48] which are commonly used for periodic systems with constant shear rate. We calculate one-body quantities such as density and current by averaging over many-body trajectories.

We obtain the steady state current and density profile by averaging 10^6 trajectory samples from a runlength of $10^3\tau$ after an initial relaxation period of 2τ. For start-up dynamics, the system is simulated in equilibrium for an initial 0.1τ, after which shear is switched on and the system is evolved for a further 0.4τ. Dynamics after switch-off are simulated initially for 1.5τ under shear, after which the shear force is switched off and the system is evolved for a further 0.1τ. In our experience, this protocol is sufficient to ensure that a steady state has been reached, given our parameters. Time-dependent current and density profiles for the dynamics in full non-equilibrium are then calculated per timestep *via* an average over 10^4 realisations.

IV. Steady state

We subject our system to a strongly inhomogeneous, but steady, square wave external force in z direction with an amplitude of $5\frac{k_{\mathrm{B}}T}{\sigma}$ and a period of 5σ (see Fig. 2). After a short time $\approx 10^{-1}\tau$, the system settles into a steady state ($\partial_t\rho = \partial_t \mathbf{J} = 0$).

This state has some interesting properties (Fig. 2, current and density profile in steady state). The BD results indicate that, even though no external force is acting in the x direction, the density profile becomes inhomogeneous. This effect is driven purely by superadiabatic forces and is thus a true non-equilibrium effect. Phenomenological approaches to incorporate such forces into DDFT have been proposed in ref. 9 and 23. Stuhlmüller *et al.*[39] have studied shear induced particle migration in a system of Gaussian core particles with PFT. In our PFT calculations, we impose the inhomogeneous density sampled in BD with a temporally constant external potential $V_{\mathrm{ext}}(x)$.

The harsh spatial step in the driving force field is reflected in the current profile: the current reverses its orientation in a region smaller than $\sigma/10$. Inside the regions of near-constant force, instead of a monotonic approach to the maximum, the current profile displays an oscillation close to the edge. The occurrence of this effect suggests a complex nonlocal interaction, supporting our corresponding approach in PFT.

Using a least-squares fit of the PFT velocity profile to the BD velocity profile, we obtain values for the shear viscosity η, as it appears in P_t^{exc}, *cf.* (19), as well as for σ_{M}, *cf.* (24); the latter variable is relevant for determining the parameters of the diffusing memory kernel K_{D} (23). Fig. 2 shows the resulting velocity profiles from PFT. In the given case, we obtain $\sigma_{\mathrm{M}} \approx \sigma/3$, which is of the order of the hard sphere radius. The effective interaction in steady state is therefore short-ranged.

While not being perfect, the agreement between BD and PFT is much better for the diffusing memory form (21) than it is for the local form (20). Perhaps contrary to intuition, the profile obtained from the local memory model is smoother and does not represent the jump in the current profile that is observed in BD. The reason for this becomes clear when considering the effect of the spatial nonlocality of K_{D}.

The velocity gradient $\partial_x v_z$ has a large spike at the jump of the velocity itself. In the local memory model, this spike contributes evenly for every point in the history of the system. In the diffusing model, it is smoothed out by the integral over x' for times $t' < t$. The penalty for a jump in the velocity is thus much lower in the diffusing model.

Since P_t^{exc} depends only on inter-particle interactions and not on external forces, and should be translationally invariant, no spatially local memory kernel can accurately represent this feature in the velocity profile, no matter how complex the temporal behaviour. In other words, spatial nonlocality is not only the most general form of memory, but it is required for the correct description of strong inhomogeneities within the velocity gradient approach.

V. Transient dynamics

We next investigate the transient dynamics into and out of the steady state. First, we address the transient going from equilibrium to a sheared system. The external shear force field is the

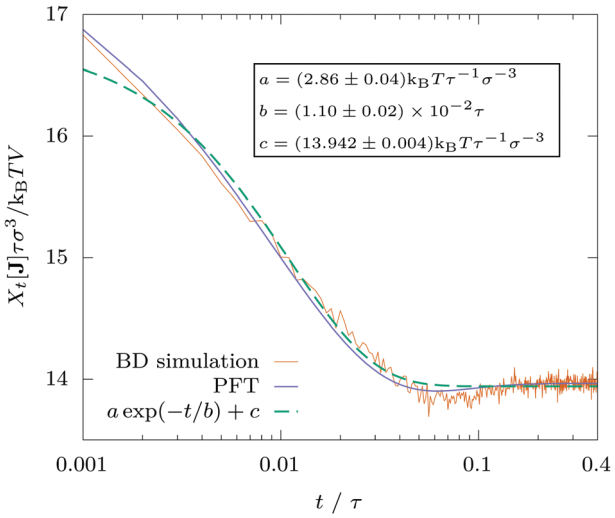

Fig. 3 Time evolution (on a logarithmic scale) of the scaled mean external power X_t per volume after switching on the shear force at $t = 0$, from BD simulation and PFT, together with a least-squares fit of a simple exponential decay $a \exp(-t/b) + c$.

same as above. It is switched on instantaneously at $t = 0$ and switched off again at a later time. The system responds instantly to the external force, with an instantaneous current profile that has larger magnitude than the steady state current. This instant response to the external force is consistent with the fact that inertia is neglected in overdamped BD. Then, viscosity slows the system down into the steady state (see Fig. 3). This process takes finite time, because the particles need to traverse, on average, the mean free path $\lambda = (\sqrt{2}\pi\rho\sigma^2)^{-1}$ between collisions,[49] which takes, with diffusive dynamics, about λ^2/D, which is $\approx 0.1\tau$ in our system.

The decay of the mean external power (15) into the steady state can be described reasonably well with an exponential decay model $X_t/V = a \exp(-t/b) + c$, where a and c are parameters with the dimension of power per volume, and b is a parameter with the dimension of a time. Physically, c can be identified as the mean steady state external power density, a as the initial mean super-steady external power density, and b as the decay time. However, the decay shows features beyond a simple exponential, which are captured by PFT with diffusing memory kernel. For times $0.05 \leq t/\tau \leq 0.1$, the external power dips below the plateau value, and the initial decay is steeper than exponential.

Next, we explore the dynamics after switching off the shear force (see Fig. 4). Surprisingly, the current does not relax

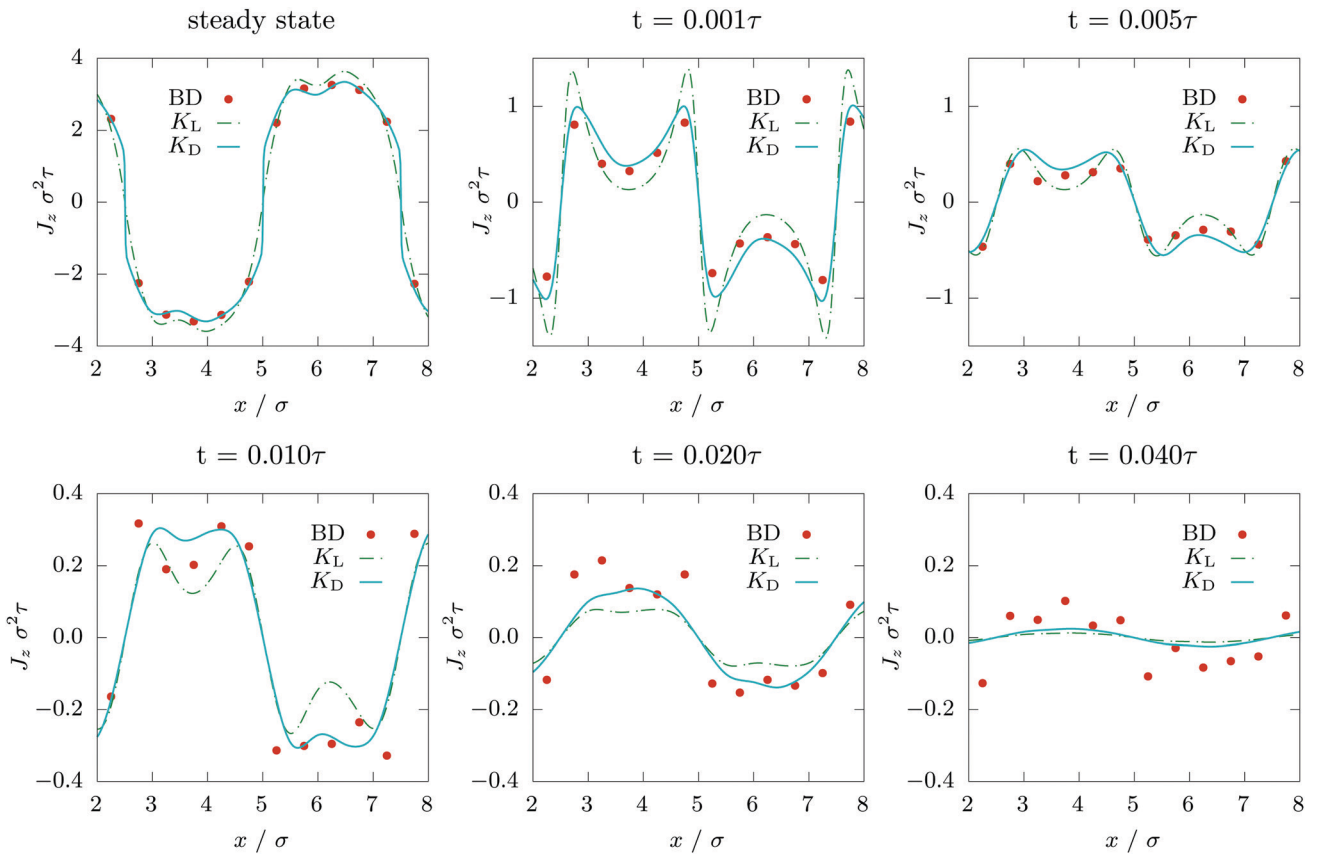

Fig. 4 Time evolution of the scaled current profile $J_x\sigma^2\tau$ as a function of x/σ after switching off the shear force at $t = 0$, obtained from BD simulation (symbols), and PFT with local memory kernel K_L (dashed line) and diffusing memory kernel K_D (solid line). The sign of the current flips globally after the shear force is switched off, followed by a decay into equilibrium. The diffusing memory model in PFT significantly outperforms the local approach in representing the BD current profiles.

monotonically into equilibrium, but rather undergoes a global reversal first, and then smoothly equilibrates. This remarkable result has perhaps been hinted at by Krüger and Brader,[23] who report "If the shear field is suddenly switched off, we find that the equilibration dynamics show an interesting symmetry with that following switch on[...]." Other than that, to the best of our knowledge, this effect has not been reported in the literature.

Using the time-dependent velocity field measured in BD for switch-on and switch-off, we can determine the remaining free parameters in K_L and K_D. The exponential decay in both K_L and K_D is one of the most simple forms of memory. Starting from an initial equilibrium state, the memory integral at time $t = 0$ vanishes, because the velocity gradient vanishes at negative times. Therefore, the superadiabatic force field is also zero just after switching on, and the current is directly proportional to the driving force. Memory then slowly builds up, with a dynamical behaviour that is governed in our approximation by the memory time τ_M. We obtain memory times of roughly $\tau_M = 0.02\tau$ for switch-on. The superadiabatic forces oppose the current, slowing the system into a steady state.

The steady state is truely reached once the current has not changed over a few memory times τ_M and thus the memory integral no longer changes. Then, the driving force can be switched off and the transient back into equilibrium can be observed. PFT accurately predicts the motion reversal observed in BD and provides an explanation: in the steady state, the force balance (*cf.* eqn (6)) includes adiabatic forces $\mathbf{f}_{ad}$, external forces $\mathbf{f}_{ext}$ and superadiabatic forces $\mathbf{f}_{sup}$. In the direction of shear, $\mathbf{f}_{ad}\cdot\hat{\mathbf{e}}_z = 0$ because of the homogeneity of ρ in z. As we know, $\mathbf{f}_{sup}$ is opposed to the external force. With $\mathbf{f}_{ext} = 0$ after switching-off, the superadiabatic excess forces still remain, because they arise from the memory integral. Thus, the superadiabatic forces become driving forces with an opposed direction of motion. The system returns to equilibrium only after the memory has cleared. The memory time obtained here is roughly $\tau_M = 0.01\tau$. While the decay of the counter-current is well described by the exponential decay memory model up until $t \approx 0.02\tau$, it seems to overestimate the rate of relaxation for later times (see Fig. 4).

VI. Conclusion

We have studied the Brownian hard sphere fluid under inhomogeneous, time-dependent shear with BD simulations and PFT. In steady state, under strongly inhomogeneous shear, spatially nonlocal memory shapes the current profile in ways spatially local memory cannot. Non-local memory is therefore required to describe general external forces acting on the fluid with a true separation of intrinsic and extrinsic effects. Exponential memory is an adequate and simple approximation that well describes nonequilibrium dynamics after switching (on and off) of an external field. The effect of motion reversal after switch-off is surprising if thought about in a microscopic picture, but has a straightforward explanation in PFT: slowing memory forces in steady state become driving forces after the shear force has been switched off. The rigorous framework of PFT is therefore an appropriate tool to gain insight into the behaviour of the Brownian hard-sphere fluid.

Non-local memory could be a relevant factor in the study of inhomogeneous colloidal systems such as colloids undergoing capillary collapse at an interface.[50] We are also interested to investigate the effect of the approximation presented here on the bulk dynamics of hard spheres, such as the van Hove correlation function, which has been studied recently experimentally and with DDFT.[51] To this end, we plan to employ PFT in the dynamic test particle limit.[21,22,52]

The excess superadiabatic functional can be further developed in two directions: spatially, structural forces can be incorporated with higher orders of the velocity gradient. The diffusing nonlocality provides good results, but has free parameters that need to be tuned by BD simulation or other benchmarks. Instead, they might be derived from the particle interaction, perhaps based on fundamental measures to allow for a deeper physical interpretation. Temporally, the exponential decay model could be improved. Research on memory in molecular dynamics provides a jumping-off point.[30] Recently, Jung *et al.*[31] presented a method to obtain memory kernels that could be adapted to our approach.

It would also be interesting to investigate the implications of the diffusing memory kernel (21) in the context of the non-equilibrium Ornstein–Zernike relation for the dynamical two-body structure.[53,54]

Finally, we expect the current reversal effect, presented here for Brownian hard spheres, to be reproducible in an experimental realisation with colloidal particles. External forces could be applied either mechanically, using a rheometer with a specifically designed geometry that approximates the step shear, or with optical methods. However, hydrodynamic interactions, which are neglected in our study, will likely induce additional effects.

Conflicts of interest

There are no conflicts of interest to declare.

Acknowledgements

We thank Daniel de las Heras for useful comments. This work is supported by the German Research Foundation (DFG) *via* SCHM 2632/1-1.

References

1 C. d. de Kruif, E. Van Iersel, A. Vrij and W. Russel, Hard sphere colloidal dispersions: Viscosity as a function of shear rate and volume fraction, *J. Chem. Phys.*, 1985, **83**, 4717.
2 L. Marshall and C. F. Zukoski, Experimental studies on the rheology of hard-sphere suspensions near the glass transition, *J. Phys. Chem.*, 1990, **94**, 1164.
3 D. R. Foss and J. F. Brady, Brownian dynamics simulation of hard-sphere colloidal dispersions, *J. Rheol.*, 2000, **44**, 629.

4 J. K. G. Dhont, M. P. Lettinga, Z. Dogic, T. A. J. Lenstra, H. Wang, S. Rathgeber, P. Carletto, L. Willner, H. Frielinghaus and P. Lindner, Shear-banding and microstructure of colloids in shear flow, *Faraday Discuss.*, 2003, **123**, 157.
5 J. K. G. Dhont and G. Nägele, Critical viscoelastic behavior of colloids, *Phys. Rev. E*, 1998, **58**, 7710.
6 M. Cates, C. Holmes, M. Fuchs and O. Henrich, Schematic mode coupling theories for shear thinning, shear thickening, and jamming, in *Unifying Concepts in Granular Media and Glasses*, ed. A. Coniglio, A. Fierro, H. Herrmann and M. Nicodemi, Elsevier, Amsterdam, 2004.
7 M. Fuchs and M. E. Cates, Integration through transients for Brownian particles under steady shear, *J. Phys.: Condens. Matter*, 2005, **17**, S1681.
8 M. Fuchs and M. E. Cates, A mode coupling theory for Brownian particles in homogeneous steady shear flow, *J. Rheol.*, 2009, **53**, 957.
9 J. M. Brader, Nonlinear rheology of colloidal dispersions, *J. Phys.: Condens. Matter*, 2010, **22**, 363101.
10 D. Leighton and A. Acrivos, The shear-induced migration of particles in concentrated suspensions, *J. Fluid Mech.*, 1987, **181**, 415.
11 J. Chakrabarti, J. Dzubiella and H. Löwen, Reentrance effect in the lane formation of driven colloids, *Phys. Rev. E*, 2004, **70**, 012401.
12 C. W. Wächtler, F. Kogler and S. H. L. Klapp, Lane formation in a driven attractive fluid, *Phys. Rev. E*, 2016, **94**, 052603.
13 J. M. Brader and M. Krüger, Density profiles of a colloidal liquid at a wall under shear flow, *Mol. Phys.*, 2011, **109**, 1029.
14 A. A. Aerov and M. Krüger, Driven colloidal suspensions in confinement and density functional theory: Microstructure and wall-slip, *J. Chem. Phys.*, 2014, **140**, 094701.
15 A. A. Aerov and M. Krüger, Theory of rheology in confinement, *Phys. Rev. E: Stat., Nonlinear, Soft Matter Phys.*, 2015, **92**, 042301.
16 H. Jin, K. Kang, K. H. Ahn and J. K. G. Dhont, Flow instability due to coupling of shear-gradients with concentration: non-uniform flow of (hard-sphere) glasses, *Soft Matter*, 2014, **10**, 9470.
17 J. Reinhardt, F. Weysser and J. M. Brader, Density functional approach to nonlinear rheology, *Europhys. Lett.*, 2013, **102**, 28011.
18 N. Koumakis, M. Laurati, A. R. Jacob, K. J. Mutch, A. Abdellali, A. B. Schofield, S. U. Egelhaaf, J. F. Brady and G. Petekidis, Start-up shear of concentrated colloidal hard spheres: Stresses, dynamics, and structure, *J. Rheol.*, 2016, **60**, 603.
19 S. Marenne, J. F. Morris, D. R. Foss and J. F. Brady, Unsteady shear flows of colloidal hard-sphere suspensions by dynamic simulation, *J. Rheol.*, 2017, **61**, 477.
20 B. J. Ackerson and P. N. Pusey, Shear-induced order in suspensions of hard spheres, *Phys. Rev. Lett.*, 1988, **61**, 1033.
21 A. J. Archer, P. Hopkins and M. Schmidt, Dynamics in inhomogeneous liquids and glasses via the test particle limit, *Phys. Rev. E*, 2007, **75**, 040501.
22 P. Hopkins, A. Fortini, A. J. Archer and M. Schmidt, The van Hove distribution function for Brownian hard spheres: Dynamical test particle theory and computer simulations for bulk dynamics, *J. Chem. Phys.*, 2010, **133**, 224505.
23 M. Krüger and J. M. Brader, Controlling colloidal sedimentation using time-dependent shear, *Europhys. Lett.*, 2011, **96**, 68006.
24 B. Metzger and J. E. Butler, Clouds of particles in a periodic shear flow, *Phys. Fluids*, 2012, **24**, 021703.
25 R. Zwanzig, Memory effects in irreversible thermodynamics, *Phys. Rev.*, 1961, **124**, 983.
26 H. Mori, Transport, collective motion, and Brownian motion, *Prog. Theor. Phys.*, 1965, **33**, 423.
27 D. E. Smith and C. B. Harris, Generalized Brownian dynamics. I. Numerical integration of the generalized Langevin equation through autoregressive modeling of the memory function, *J. Chem. Phys.*, 1990, **92**, 1304.
28 P. Szymczak and B. Cichocki, Memory effects in collective dynamics of Brownian suspensions, *J. Chem. Phys.*, 2004, **121**, 3329.
29 J.-D. Bao, P. Hänggi and Y.-Z. Zhuo, Non-markovian Brownian dynamics and nonergodicity, *Phys. Rev. E*, 2005, **72**, 061107.
30 D. Lesnicki, R. Vuilleumier, A. Carof and B. Rotenberg, Molecular hydrodynamics from memory kernels, *Phys. Rev. Lett.*, 2016, **116**, 147804.
31 G. Jung, M. Hanke and F. Schmid, Iterative reconstruction of memory kernels, *J. Chem. Theory Comput.*, 2017, **13**, 2481.
32 A. Scala, T. Voigtmann and C. De Michele, Event-driven Brownian dynamics for hard spheres, *J. Chem. Phys.*, 2007, **126**, 134109.
33 M. Schmidt and J. M. Brader, Power functional theory for Brownian dynamics, *J. Chem. Phys.*, 2013, **138**, 214101.
34 U. M. B. Marconi and P. Tarazona, Dynamic density functional theory of fluids, *J. Chem. Phys.*, 1999, **110**, 8032.
35 A. J. Archer and R. Evans, Dynamical density functional theory and its application to spinodal decomposition, *J. Chem. Phys.*, 2004, **121**, 4246.
36 A. Fortini, D. de las Heras, J. M. Brader and M. Schmidt, Superadiabatic forces in Brownian many-body dynamics, *Phys. Rev. Lett.*, 2014, **113**, 167801.
37 D. Stopper, K. Marolt, R. Roth and H. Hansen-Goos, Modeling diffusion in colloidal suspensions by dynamical density functional theory using fundamental measure theory of hard spheres, *Phys. Rev. E*, 2015, **92**, 022151.
38 D. Stopper, R. Roth and H. Hansen-Goos, Dynamical density functional theory for dense suspensions of colloidal hard spheres, *J. Chem. Phys.*, 2015, **143**, 181105.
39 N. C. X. Stuhlmüller, T. Eckert, D. de las Heras and M. Schmidt, Structural nonequilibrium forces in driven colloidal systems, *Phys. Rev. Lett.*, 2018, **121**, 098002.
40 D. de las Heras and M. Schmidt, Velocity gradient power functional for Brownian dynamics, *Phys. Rev. Lett.*, 2018, **120**, 028001.
41 P. Krinninger and M. Schmidt, Power functional theory for active Brownian particles: General formulation and power sum rules, *J. Chem. Phys.*, 2019, **150**, 074112.

42 D. de las Heras, J. Renner and M. Schmidt, Custom flow in overdamped Brownian dynamics, *Phys. Rev. E*, 2019, **99**, 023306.
43 R. Evans, The nature of the liquid-vapour interface and other topics in the statistical mechanics of non-uniform, classical fluids, *Adv. Phys.*, 1979, **28**, 143.
44 N. D. Mermin, Thermal properties of the inhomogeneous electron gas, *Phys. Rev.*, 1965, **137**, A1441.
45 Y. Rosenfeld, Free-energy model for the inhomogeneous hard-sphere fluid mixture and density-functional theory of freezing, *Phys. Rev. Lett.*, 1989, **63**, 980.
46 S. G. Johnson, The nlopt nonlinear-optimization package, http://ab-initio.mit.edu/nlopt.
47 M. J. Powell, A direct search optimization method that models the objective and constraint functions by linear interpolation, *Advances in optimization and numerical analysis*, Springer, 1994, pp. 51–67.
48 A. W. Lees and S. F. Edwards, The computer study of transport processes under extreme conditions, *J. Phys. C*, 1972, **5**, 1921.
49 J.-P. Hansen and I. R. McDonald, *Theory of Simple Liquids*, Academic Press, Oxford, 4th edn, 2013.
50 J. Bleibel, S. Dietrich, A. Domínguez and M. Oettel, Shock waves in capillary collapse of colloids: A model system for two-dimensional screened Newtonian gravity, *Phys. Rev. Lett.*, 2011, **107**, 128302.
51 D. Stopper, A. L. Thorneywork, R. P. A. Dullens and R. Roth, Bulk dynamics of Brownian hard disks: Dynamical density functional theory versus experiments on two-dimensional colloidal hard spheres, *J. Chem. Phys.*, 2018, **148**, 104501.
52 J. M. Brader and M. Schmidt, Power functional theory for the dynamic test particle limit, *J. Phys.: Condens. Matter*, 2015, **27**, 194106.
53 J. M. Brader and M. Schmidt, Nonequilibrium Ornstein-Zernike relation for Brownian many-body dynamics, *J. Chem. Phys.*, 2013, **139**, 104108.
54 J. M. Brader and M. Schmidt, Dynamic correlations in Brownian many-body systems, *J. Chem. Phys.*, 2014, **140**, 034104.

